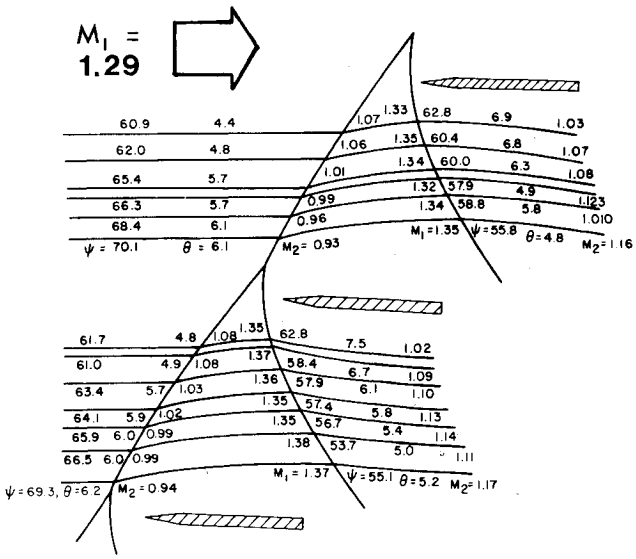

Fig. 5 Flowfield determination of PHSSVC in PHSST at $M_1 = 1.29$, incidence = 1.75 deg.

Kodabromide F5 high-contrast photographic paper in a developer solution of two parts water to one part Dektol.

A standard test proceeded as follows: After the tunnel was started, the total pressure rake was moved to a predetermined location. Total pressure readings were then taken off a mercury manometer board (within ±2.5 mm Hg accuracy) and a shadowgraph was taken. The smoke generator was then started and smoke entered the test section. Smoke photo exposure times varied from 1/10th to 1/50th s at aperture settings from *f*4.5 to *f*8.0. After this, the pitot rake was moved to another position and the procedure repeated until all appropriate probe positions were examined. The smoke and shadowgraph negatives for each probe position were both enlarged to the same scale and superimposed on each other. This procedure assumes steady flow and has produced good results. From these enlargements, the shock inclination and streamline deflections were measured optically and graphically to within ± 1 deg.

Although the major goal of this testing program is to prove the applicability of this technique to cascades,.it was felt the concept should be proven first using simpler geometries. Therefore, a number of two-dimensional shapes were tested, such as a cylinder, various wedge and flat-top airfoils, and a Whitcomb supercritical wing section. These tests indicated that the method was reliable for oblique and curved shocks. An example is shown in Fig. 2, which is a comparison of total pressure ratio across the curved bow shock of a circular cylinder measured by a total pressure probe and the smoke visualization technique. As can be seen, the data correlate well. Further results are given in Ref. 2.

The cascade test configuration was the Preliminary High-Speed Smoke Visualization Cascade (PHSSVC) and is seen in silhouette in Fig. 3. It consisted of seven flat plates with a leading-edge, double-wedge angle of 16 deg. The chord length is 1.27 cm with a thickness-to-chord ratio of 5%, stagger angle of 30.5 deg, solidity of 0.62, and aspect ratio of 3.0.

Results

Figure 4 is a composite photograph of transonic flow in the PHSSVC. In it the smokelines can be seen being deflected upward through the front shock, curving as the gas is re-expanded up to the passage shock where the smokelines are deflected downward to the near-axial direction. A series of oblique shocks emanating from the blunt trailing edges of the blades can also be seen. However, these will be extremely weak, as indicated by their low wave angles and small deflections, and were not studied. From a series of photographs, such as Fig. 4, the flowfield determination of Fig. 5 was made. From this, the inlet shock total pressure ratio can be isolated and the shock loss coefficient calculated. More detailed results are presented in Ref. 2.

Conclusions

This combined visualization technique should prove useful in examining the flow through the leading-edge regions of transonic cascades and make it possible to isolate the shock loss from the end-wall and profile losses.

Acknowledgment

This work was sponsored in part by the Fan and Compressor Branch of the NASA/Lewis Research Center, under Grant MSG-3133.

References

[1] Shapiro, A. H., *The Dynamics and Thermodynamics of Compressible Fluid Flow*, Vol. 1, Roland Press Company, New York, 1953, p. 529.

[2] Slovisky, J. A., Roberts, W. B., and Crouse, J. A., "High Speed Smoke Visualization for the Determination of Cascade Shock Losses," AIAA Paper 79-0042, New Orleans, La., Jan. 1979.

[3] Goddard, V. P., McLaughlin, J. A., and Brown, F. N. M., "Visual Supersonic Flow Patterns by Means of Smoke Lines," *Journal of the Aerospace Sciences*, Vol. 26, Nov. 1959, pp. 761-762.

[4] Holman, J. P., *Experimental Methods for Engineers*, McGraw-Hill Book Co., Inc., New York, 1978, p. 438.

[5] Wisler, D. C., "Shock Wave and Flow Velocity Measurements in a High Speed Fan Rotor Using the Laser Velocimeter," ASME Paper 76-GT-49, March 1976.

Thermal Analysis of a Conical Cathode of an MPD Arc

R. C. Mehta*

Vikram Sarabhai Space Centre, Trivandrum, India

Nomenclature

Bi = Biot number = hL/k, nondimensional
h = heat-transfer coefficient
I = applied current
j = current density
k = thermal conductivity
L = cathode length
Q_s = heat transfer to cathode root
Q_0 = heat transfer to cathode coolant water
r = cathode radius
r_0 = cathode tip radius
T = local temperature of cathode at x
T_s = cathode temperature at $X = 0$
T_0 = cooling water temperature at $X = 1$
T_∞ = surrounding temperature
x = space coordinate
X = nondimensional length, x/L
X_1 = nondimensional conical length of cathode, L_1/L
α = semicone angle
ϵ = emissivity
θ = nondimensional temperature, T/T_s
ρ = electrical resistivity
σ = Stefan-Boltzmann constant

Received Feb. 15, 1979; revision received May 8, 1979.

Index categories: Electric and Advanced Space Propulsion; Plasma Dynamics and MHD; Radiation and Radiative Heat Transfer.

*Engineer, Propulsion Engineering Division (PSN).

Introduction

THE cathode electrode, where the transition between metallic and gaseous conduction occurs, presents a number of physical phenomena which, despite intensive investigations, both experimentally[1,2] and theoretically,[3] have defied complete understanding. The conditions in the cathode region are defined less clearly than those in the arc column,[4] which is the region of gaseous conduction well away from the cathode-fall region. The cathode must be maintained at high temperatures for emission of electrodes with moderate electric field, while undergoing minimum surface erosion. A knowledge of the temperature distribution along the cathode is, therefore, necessary for the design of the cathode configuration.

Shih et al.[5] have not considered conical shape of the cathode in their analysis of heat conduction problem with radiation and also its effect on the temperature profile. In practice, a 2% thoriated tungsten cathode whose $L/(2r)$ ratio varies from 1.5 to 3 with a semicone angle of 15-30 deg (see Fig. 1) is commonly employed in cascade and MPD arc devices.[5-8] Unfortunately no exact solution is possible for this problem, owing to the complexity of the geometry and the nonlinearity of the differential equation. To the author's knowledge, even a numerical solution has not yet been reported in the literature.

It is the purpose of this Note to develop a simple numerical solution of the energy equation that will be useful for studying the effect of geometrical parameters and Ohmic heating on the temperature distribution along the cathode.

Analysis

Consider a one-dimensional cathode of conical shape with constant thermophysical properties. The nondimensional energy equation with combined conduction, Ohmic heating, radiation, and convection can be written as

$$\frac{d^2\theta}{dX^2}+\frac{2\tan\alpha}{(X\tan\alpha+r_0/L)}\frac{d\theta}{dX}+\frac{I^2\rho}{kT_s[\pi(X\tan\alpha+r_0/L)]^2}-\frac{2\epsilon\sigma LT_s^3\tan\alpha}{k(X\tan\alpha+r_0/L)}[\theta^4-(T_\infty/T_s)^4]-\frac{2Bi\tan\alpha}{(X\tan\alpha+r_0/L)}[\theta-(T_\infty/T_s)]=0,\quad 0<X\le X_1 \tag{1a}$$

$$\frac{d^2\theta}{dX^2}+\frac{I^2\rho}{kT_s(\pi r/L)^2}-\frac{2\epsilon\sigma L^2T_s^3}{kr}\left[\theta^4-\left(\frac{T_\infty}{T_s}\right)^4\right]-\frac{2LBi}{r}\left[\theta-\left(\frac{T_\infty}{T_s}\right)\right]=0,\quad X_1<X<1 \tag{1b}$$

with the boundary conditions

$$\theta=1 \text{ at } X=0 \text{ and } \theta=(T_0/T_s) \text{ at } X=1 \tag{1c}$$

The numerical integration of this equation is facilitated by the introduction of the transformation

$$Y_1=\theta \text{ and } Y_2=(d\theta/dX)$$

The problem is, thus, reduced to the solution of the following four simultaneous equations:

For $0<X\le X_1$:

$$\frac{dY_1}{dX}=Y_2 \tag{2a}$$

$$\frac{dY_2}{dX}=-\frac{2\tan\alpha}{(X\tan\alpha+r_0/L)}Y_2-\frac{I^2\rho}{kT_s[\pi(X\tan\alpha+r_0/L)]^2}+\frac{2\epsilon\sigma LT_s^3\tan\alpha}{k(X\tan\alpha+r_0/L)}\left[Y_1^4-\left(\frac{T_\infty}{T_s}\right)^4\right]+\frac{2Bi\tan\alpha}{(X\tan\alpha+r_0/L)}\left[Y_1-\left(\frac{T_\infty}{T_s}\right)\right] \tag{2b}$$

For $X_1<X<1$:

$$\frac{dY_1}{dX}=Y_2 \tag{2c}$$

$$\frac{dY_2}{dX}=-\frac{I^2\rho}{kT_s(\pi r/L)^2}+\frac{2\epsilon\sigma L^2T_s^3}{kr}\left[Y_1^4-\left(\frac{T_\infty}{T_s}\right)^4\right]+\frac{2BiL}{r}\left[Y_1-\left(\frac{T_\infty}{T_s}\right)\right] \tag{2d}$$

This set of first-order equations is readily solved with a standard fourth-order Runge-Kutta numerical solution technique. It is possible to solve the problem as an initial value problem starting at $X=0$ and by initiating the calculation with trial values of $[dY_1/dX]_{X=0}$. The solution is obtained by an iterative satisfaction of the boundary condition at $X=1$. A FORTRAN IV computer program has been prepared for the calculation of temperature distribution along the cathode. The computations have been performed on an IBM 360/44 digital computer for applied current strength of 0-1000 A, for cathode length of 2.54 cm, radius of 0.3 and 0.476 cm, semicone angles of 15 and 30 deg and heat-transfer coefficient[9] equal to 100 W/m^{2}K. For computational purposes, $T_s=3000$ K has been selected, which is below the melting point of tungsten.[5] T_0 and T_∞ are taken as 300 and 450 K, respectively. The material properties are $\epsilon=0.4$, $k=110$ W/mK (Ref. 5), and $\rho=55\times10^{-8}$ Ω − m (Ref. 10).

Results and Discussions

Numerical results of the computations are presented in Figs. 2 and 3. Temperature distributions along the cathode for

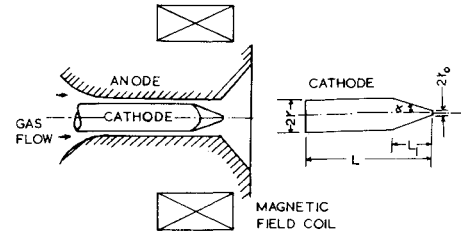

Fig. 1 MPD arcjet and cathode used.

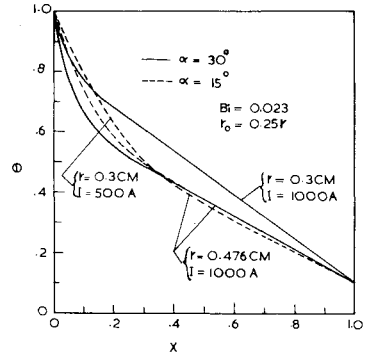

Fig. 2 Cathode temperature profiles.

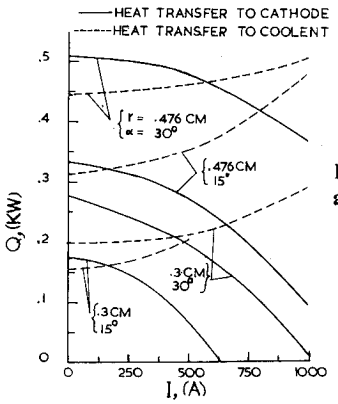

Fig. 3 Heat transfers to cathode and to coolant vs applied current.

$r=0.3$ and 0.476 cm, $\alpha=15$ and 30 deg are depicted in Fig. 2. It is seen that temperature decreases rapidly along the nosecone portion of the cathode ($0\leq X\leq X_1$), while in the remaining length of the cathode ($X_1\leq X\leq 1$), the temperature varies almost linearly. The decrease in α increases the electrical resistance due to the decrease in the cross-sectional area in the nosecone portion of the cathode. However, it is found that numerical instability occurs for $r=0.3$ cm at $I>500$ A and $\alpha=15$ deg and also at $I>1000$ A and $\alpha=30$ deg. This numerical instability is attributed to overheating of the cathode root by Joule's heating when the current exceeds the above values. Figure 3 shows the variation of Q_s and Q_0 as a function of applied current. It is interesting to note that as current increases, heat transfer to cathode coolant increases, while heat transfer to cathode tip decreases rapidly and reaches to zero value at the point where the numerical instability is noticed in the computations. It can be concluded, therefore, that for $I<500$ A, a small diameter and small semicone angle of cathode is economical, owing to less heat transfer to coolant, while $I>500$ A, a larger diameter, and short nosecone length of cathode is favorable in order to prevent melting of the cathode tip due to excessive Ohmic heating. It would be worthwhile to mention here that the characteristic cathode voltage $U_c(=Q_s/I)$ decreases with increasing arc current, while heat transfer to the cathode coolant increases with increasing arc current, as shown in Fig. 3. This is very similar to the trend observed by conventional experiments on an MPD arc.[5]

At the cathode the electron component has to satisfy the appropriate emission law. It would be inappropriate to discuss electron emission theories here. However, it is sufficient to mention that a theory of thermionic emission under the influence of high temperature has been developed by Richardson.[11] The expression for current density can be written as

$$j=AT^2\exp(-b/T) \tag{3}$$

where A and b are constants[11] and T is cathode temperature.

For the sake of brevity, we are not presenting the current density profile along the cathode. Integration of Eq. (3) over the cathode surface yields a value of total discharge current from cathode to arc. Using thermionic relation only, 70-85% current continuity condition is satisfied at the cathode root. In order to satisfy current continuity condition precisely one has to take into consideration the combined effect of thermionic and field emission in computation of current density profile along the cathode and also higher cathode tip temperature.

One disadvantage of invoking the numerical analysis is that the results do not give a clear functional relation among the arc current density and temperature at the cathode root vs cathode geometrical configuration. The following simple procedure may be adopted for computational purposes in the thermal design of the cathode:

1) Select the primary cathode geometrical configuration from Fig. 3 for a given value of applied current.

2) Satisfy the current continuity condition by taking into account thermionic and field emission expressions. If the desired accuracy is not achieved, change the geometrical parameters or cathode tip temperature or both and solve Eqs. (2) to obtain temperature distribution along cathode.

3) Repeat the preceding steps until the current continuity condition satisfies a given limit of tolerance.

References

[1] Malliaris, A. C., "Phenomena in the Cathode Region of an MPD Accelerator," *AIAA Journal*, Vol. 5, July 1967, pp. 1325-1328.

[2] Turchi, P. J. and John, R. G., "Cathode Region of a Quasi-Steady MPD Arc Jet," *AIAA Journal*, Vol. 9, July 1971, pp. 1372-1379.

[3] Lee, T. H., Greenwood, A., Breingan, W. D., and Fullerton, H. P., "Voltage Distribution, Ionization, and Energy Balance in the Cathode Region of an Arc," ARL 64-152, Office of Aerospace Research, Wright-Patterson AFB, Ohio, Oct. 1964.

[4] Mehta, R. C., "Theoretical Analysis of Constricted Electric Arc by Iteration Method," *Journal of Applied Physics*, Vol. 50, June 1979, pp. 4453-4456.

[5] Shih, K. T., Pfender, E., and Eckert, E.R.G., "Thermal Analysis of Cathode and Anode Regimes of an MPD Arc," NASA CR 54664, Jan. 1968.

[6] Emmons, H. W., "Recent Development in Plasma Heat Transfer," *Modern Development in Heat Transfer*, Academic Press, New York, 1963, pp. 401-478.

[7] Donskoi, A. V., Klubrikin, V. S., and Parkhomenko, A. S., "The Effect of Arc Length on the Electrical Characteristics of a Plasmatron," *High Temperature*, Vol. 8, May-June 1970, pp. 461-465.

[8] Olsen, H. N., "Determination of Properties of an Optically Thin Argon Plasma," *Temperature, Its Measurement and Control in Science and Industry*, Vol. III, Part 1, C. M. Herzfeld, ed., Reinhold Publishing Corp., New York, 1972.

[9] Eckert, E.R.G. and Drake, R. M., *Analysis of Heat and Mass Transfer*, McGraw Hill Book Co., Inc., New York, 1972.

[10] *Standard Handbook for Electrical Engineering*, 9th Ed., McGraw Hill Book Co., Inc., 1957, p. 478.

[11] Cobine, J. D., *Gaseous Conductor*, Dover Publication Inc., New York, 1958, pp. 106-122.

Modal Analysis of the Transient Asymmetric Response of Thin Circular Plates

H. D. Fisher*
Combustion Engineering, Inc., Windsor, Conn.

Introduction

SCHLAK et al[1] have presented a general integral solution for the free and forced response of an elastically supported, thin circular plate subjected to a time-dependent surface load. The generalized theory contained in Ref. 1 encompasses the axisymmetric analysis of Weiner[2] which was corrected by Fisher.[3] An attempt to derive the equations governing the axisymmetric plate response to a concentrated central loading from the general solution of Ref. 1 has disclosed that three of the equations contained in Ref. 1 are incorrect.

The objectives of this Note are to: 1) indicate the corrections required in the section of Ref. 1 entitled General Analysis, 2) compare the transient deflection histories from

Received Feb. 27, 1979; revision received May 7, 1979.

Index category: Structural Dynamics.

*Consulting Engineer, Reactor Engineering Dept.